Article

Atomic Structure Modeling of Multi-Principal-Element Alloys by the Principle of Maximum Entropy

Shaoqing Wang

Shenyang National Laboratory for Materials Science, Institute of Metal Research, Chinese Academy of Sciences, Shenyang 110016, China; E-Mail: sqwang@imr.ac.cn; Tel.: +86-24-23971842

Abstract: Atomic structure models of multi-principal-element alloys (or high-entropy alloys) composed of four to eight componental elements in both BCC and FCC lattice structures are built according to the principle of maximum entropy. With the concept of entropic force, the maximum-entropy configurations of these phases are generated through the use of Monte Carlo computer simulation. The efficiency of the maximum-entropy principle in modeling the atomic structure of random solid-solution phases has been demonstrated. The bulk atomic configurations of four real multi-principal-element alloys with four to six element components in either BCC or FCC lattice are studied using these models.

1. Introduction

The discovery of high-entropy alloys [1,2] renewed people's understanding of the importance of entropy in the structure formation of solid state matter. The concept of entropy was introduced by Clausius in 1865 [3]. Boltzmann gave a theoretical explanation for entropy from the viewpoint in microscopic scale [4]. By definition, entropy is a measure of disorder, randomness, or multiplicity in a physics system. The condition of thermodynamic equilibrium for a condensed-mater system is given by the minimization of Gibbs free energy, $G = U + PV - TS$, where U, S, P, V and T are the internal energy, entropy, pressure, system volume, and temperature, respectively. Particle systems composed of atoms, ions, or molecules can exist in various states from gas, liquid to solid under different

temperature and pressure conditions. The structure stability of a solid phase is closely related with its surrounding environment. A stable phase at high temperature can be unstable or metastable in low temperature, and *vice versa*. Under ambient atmospheric pressure conditions, the internal energy and the entropy of a system are the two important factors of phase stability at a finite temperature, especially entropy which acts the leading role under high temperature conditions. The formation of solid solutions in multi-component high-entropy alloys originates from the high value of their mixed/configurational entropy as the alloy solidifies [1]. The higher the configurational entropy, the easier the formation of random solution phases at high temperatures. Therefore, it is essential to explore the atomic structures characterized by the maximum entropy for these unique alloys having random solid solutions.

High-entropy alloys generally contain five or more componential elements in nearly equimolar composition [1,5–7]. In this respect, high-entropy alloys are also called multi-principal-element (MPE) alloys. The successful experimental preparation of quaternary high-entropy alloys with compositions of WNbMoTa [8] and FeCoCrNi [9] were reported. It is astonishing that some high-entropy alloys possess quite simple lattice structures, despite their highly complicated elemental compositions. These alloys are found greatly to favor close-packed and disordered crystal structures. The most commonly seen structure patterns of high-entropy alloys form body centered cubic (BCC) [1,6–9] or face centered cubic (FCC) [1,5,7] lattices. High-entropy alloys with hexagonal close packing (HCP) structure have been predicted theoretically, but have not yet been realized experimentally .

The principle of maximum entropy (MaxEnt) is a combinatorial theory comprising Shannon's entropy in information theory [10] and the Boltzmann-Gibbs entropy in statistical mechanics for estimating probability distribution from a few limited pieces of information [11]. It uses a variational method for the analysis of complicated systems. In physics, the particle distribution of maximum entropy corresponds to the macrostate that has the most microstates. The successes of the MaxEnt principle have been demonstrated in various applications in the study of condensed matters [12–17].

In this work we build atomic structure models of bulk MPE alloys with BCC and FCC lattices for compositions ranging from four to eight principal elements according to the MaxEnt principle. The entropic force for the particle distribution in a closed system is defined. The MaxEnt configuration is generated by Monte Carlo simulation through entropic force minimization. Based on the built models, the atomic structure features of bulk MPE alloys are analyzed. The optimized lattice structures and lattice distortion parameters of several real quaternary, quinary, and senary MPE alloys are obtained using the models built in this work.

2. Method and Algorithm in Model Building

The entropy of an alloy system mainly consists of four parts: electronic entropy, magnetic entropy, vibrational entropy and configurational entropy or entropy of mixing. The electronic entropy is caused by the variation of electron distribution with structure configuration and temperature. The contribution of electronic entropy to the system free energy is usually very small. Alloys with iron, nickel, and cobalt elements may have magnetic entropy. The magnetic entropy describes the change of material magnetization with temperature and magnetic field [18]. Material magnetization goes to zero at very high temperature, therefore the effect of magnetic entropy on the formation of random solid

solutions can be omitted. The vibrational entropy comes from the lattice vibration of atoms in a solid under finite temperature conditions. The configurational entropy is related to the number of possible configurations of a system. Besides, there is zero point entropy in solids. Zero point entropy arises from the existence of the frozen-in phase which is stable at higher temperature and is not able to reach real thermal equilibrium as the material cools to 0 K [19]. The configurational entropy of high-entropy alloy molten solutions or melts plays the decisive role in the structure formation of this kind of novel alloy.

The configurational entropy of multi-component alloy melt is very like the entropy of mixing in ideal gases. Like the mixing entropy of ideal gases, the configurational entropy of *n*-component alloy melt is defined by:

$$S_{conf} = -R\sum_{i=1}^{n} x_i \ln(x_i), \tag{1}$$

where x_i is the molar concentration of the ith element which satisfies the following equation:

$$\sum_{i=1}^{n} x_i = 1, \tag{2}$$

R is the gas constant. It should be noted that Equation (1) is also valid for random solid solutions of a multi-component alloy.

A Lagrangian equation can be constructed from Equations (1) and (2) according to the MaxEnt principle [10]:

$$L(x) = -R\sum_{i=1}^{n} x_i \ln(x_i) + \lambda(\sum_{i=1}^{n} x_i - 1). \tag{3}$$

Taking the derivative of *L(x)* with respect to x_i and set $\partial L(x)/\partial x_i = 0$, one has:

$$-R\ln(x_i) - R - \lambda = 0. \tag{4}$$

The x_i, for the maximum entropy distribution, is solved from Equation (4):

$$x_i^* = \exp(-\frac{R+\lambda}{R}). \tag{5}$$

Noticing that $\sum_{i=1}^{n} x_i^* = 1$, one finally gets the condition of molar concentration under the maximum configurational entropy for a *n*-component alloy to be:

$$x_i^* = \frac{1}{n}, \tag{6}$$

i.e., all the componential elements should have the equimolar concentration.

The free space of a particle is defined as its maximum non-overlapping space with the other particles. We define v_i as the free space of the particle *i* for a system with *N* identical particles in space *V*. Following the above procedure, it is easy to prove that $v_i = V/N$ under the MaxEnt condition, *i.e.*, the identical particles should have the equal maximum free space *V/N* within the limitation of maximum entropy. This is a state of uniform spatial distribution of particles. Therefore, the maximum entropy state has the configuration with a uniform particles distribution over the system.

According to the MaxEnt principle, every particle is striving for the maximum free space in the system. The driving force for this trend is called as the entropic force. The definition of the entropic force is given by [20,21]:

$$\boldsymbol{F}(\boldsymbol{X}) = T\nabla_X S(\boldsymbol{X}), \tag{7}$$

where T is temperature, $S(X)$ is the entropy under the system configuration $\boldsymbol{X}$. Since there is a proportional relationship between entropy and the particle's free space for a closed particle system with a fixed volume V, the contribution of particle i to the system entropy can be written as:

$$s_i(\boldsymbol{r}) = kv_i(\boldsymbol{r}), \tag{8}$$

where $v_i(\boldsymbol{r})$ is the free space of particle i at position $\boldsymbol{r}$, k is a constant. Derived from Equations (7) and (8), the entropic force $f_i(r)$ on particle i is given by:

$$\boldsymbol{f}_i(\boldsymbol{r}) = kT\nabla_r v_i(\boldsymbol{r}). \tag{9}$$

Equation (9) indicates that the entropic force $f_i(r)$ is pointed to the direction of $v_i(r)$ increase. Hence, the MaxEnt configuration can be reached through minimizing $f_i(r)$ or maximizing $v_i(r)$ for each particle in the system.

3. Results and Analyses

3.1. Binary Alloys

The atomic structure models of BCC binary random-substitution alloys $Fe_{1-x}Cr_x$ (x = 0.085, 0.111, 0.206) are created to illustrate the MaxEnt algorithm for the atomic structure modeling of MPE alloys in the follows.

A n × n × n BCC lattice of Fe matrix is created firstly. Then, the Fe atoms at some random sites are replaced by the solute atoms Cr. In the next step, this initial configuration is optimized according to the MaxEnt principle in the following way: The state of the maximum system entropy for this binary phase should be that each of Cr atom approaches to its maximum free space. Let r_0^i to be the distance of atom i to its nearest same-element neighbor and $r_f = r_0^i /2$, the volume of the atom's free space can be approximately calculated by $v_i = 4\pi r_f^3 /3$. As for a system with particles in a closed space, the maximum free space means that there is no any other same-element atom within this range. This condition for a solid solution is equivalent to that where all solute atoms should be separated as far as possible. A Monte Carlo simulation code in Python language [22], numerically enhanced by NumPy [23], was developed to perform the maximum-entropy optimization for the above initial random configuration. The main part of the optimization program is constituted by a big repeat loop. The neighboring *status quo* of the solute atom i is analyzed at first in each loop, then the code invokes a Monte Carlo routine to seek a possible position replacement of solute atom i with a Fe solvent atom through random sampling algorithm. The position-replacing action is executed only when the distance of solute atom i, at the new position, to its nearest solute neighbor becomes longer than at its original one. The solute Cr atoms are restricted to replace the Fe atom only on the strict BCC lattice sites during the optimization process. The loop terminates until the MaxEnt

condition is satisfied. Our created $4 \times 4 \times 4$ atomic structure models of binary alloys $Fe_{1-x}Cr_x$ are illustrated in Figure 1.

Figure 1. $4 \times 4 \times 4$ atomic structure models of binary alloys $Fe_{1-x}Cr_x$. The ratios of solute to solvent atoms in Figure 1a to 1c are 16:173, 21:168, and 39:150, respectively. Cr atoms (black balls) are dispersed in the Fe (transparent balls) solvent matrix.

| (a) | (b) | (c) |
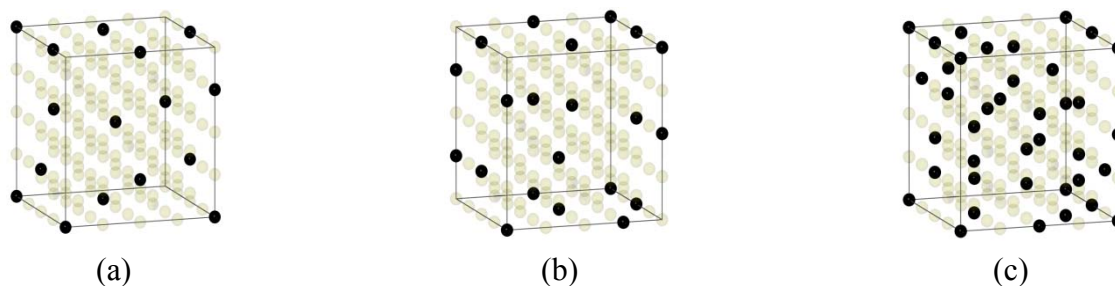
The created models are carefully examined to assess the degree of compliance with the MaxEnt principle. The results of model structure analysis are given in Table 1. The table shows that the averaged distance to the nearest neighbors, $\overline{r_0}$, monotonically decreases with the increase of solute atoms which is in consistent with the fixed model volume. Δr gives the difference between the maximum r_{min} and minimum r_{max} distances for the nearest neighbors among solute atoms. The smaller the value, the more uniform the distribution of the solute atoms. It was suggested that the random packing of hard spheres in three dimensional space has a density limit between 55.5% [24] and 63.4% [25]. The packing density of the atoms' free-space balls in our built models is a little smaller than the low limit. The main reason can be understood from the fact that there is a BCC lattice-site restriction for the positions of solute atoms in the built models which reduces the packing efficiency to a certain extent. Another reason can be attributed to the small model size.

Table 1. Structure analysis of $Fe_{1-x}Cr_x$ models. The length unit is the lattice constant a_0 of FeCr alloys.

| Phase	$\overline{r_0}$	r_{min}	r_{max}	Δr	Density (%)
$Fe_{0.915}Cr_{0.085}$	2.2361	2.2361	2.2361	0.0000	52.6
$Fe_{0.889}Cr_{0.111}$	2.0684	2.0000	2.1795	0.1795	54.3
$Fe_{0.794}Cr_{0.206}$	1.4705	1.4142	1.6583	0.2441	52.0

3.2. BCC Multi-Principal-Element Alloys

Bulk atomic structure models of BCC MPE alloys for compositions from four to eight componential elements were created in this study. These models can be used in the studies for any four- to eight-element MPE alloys through appropriate element substitution. Since there is not a major element to act as solvent in MPE alloys, all atoms from the componential elements were randomly filled up in a cubic box by a n × n × n BCC lattice at the beginning of the model building. Then these atoms undergo distribution optimization according to the MaxEnt principle for the configuration with their maximum free space, *i.e.*, all the same-element atoms should be separated as far as possible. Here, unlike the case of a binary phase, the condition for different-type atoms replacement is that the sum of the distances

for the two replacing atoms to their nearest same-element neighbors should be increased, and no any neighboring-distance decrease should be caused after the replacement. There could be a small deviation from the equimolar concentration for some elements in the model owing to the limitation of total lattice-site number in a n × n × n BCC box. The influence of this deviation to the final model structure can be omitted for this negligible composition fluctuation (within 1.0%).

Figure 2 graphically illustrates some representative models selected from each type of these MPE phases. The information on the structure analyses of these models is presented in Table 2. The shortest distance of an atom is the distance of the atom to its nearest same-element atom. The table shows that same-elements as the first nearest neighbor can all be avoided for those BCC MPE phases with five or more elements in our MaxEnt models. Most of the same elements in quaternary and quinary BCC MPE phases are in the second nearest neighborship. This peak area moves to the third nearest neighbor as the element number increases. The uniform elemental distributions in these models are verified by the fact that the shortest distances between most of the same elements are located in a narrow range.

Figure 2. Atomic structure models of four- to eight-element BCC MPE phases by MaxEnt method. (**a**) 8 × 8 × 8 quaternary phase, (**b**) 8 × 8 × 8 quinary phase, (**c**) 8 × 8 × 8 senary phase, (**d**) 8 × 8 × 8 septenary phase, (**e**) 8 × 8 × 8 octonary phase.



(a)   (b)   (c)   (d)   (e)
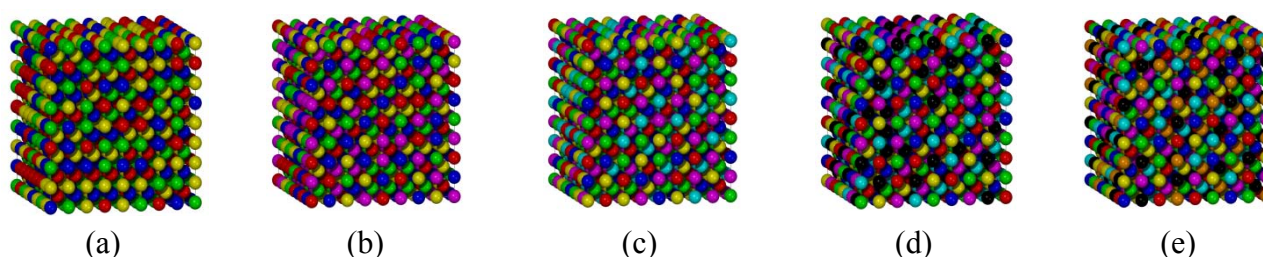
Table 2. Distribution of the shortest distances between the same-element atoms on the nearest neighbor lattice sites in the created BCC and FCC MaxEnt models. The distances for the successive nearest neighbor sites in BCC and FCC lattices are $\sqrt{3}a_0/2$, a_0, $\sqrt{2}a_0$,...; and $\sqrt{2}a_0/2$, a_0, $\sqrt{3/2}a_0$,..., respectively.

| Phase	Cell type	Distance distribution in nearest neighbor sites (%)					
		1	2	3	4	5	6
Quaternary phase	BCC	8.5	83.0	6.9	1.6	0.0	0.0
	FCC	74.3	23.8	1.9	0.0	0.0	0.0
Quinary phase	BCC	0.0	65.5	30.6	3.4	0.5	0.0
	FCC	47.3	45.0	7.5	0.2	0.0	0.0
Senary phase	BCC	0.0	41.4	52.4	6.0	0.2	0.0
	FCC	17.2	64.9	17.7	0.2	0.0	0.0
Septenary phase	BCC	0.0	19.2	65.3	15.0	0.3	0.2
	FCC	3.9	50.4	44.4	1.1	0.2	0.0
Octonary phase	BCC	0.0	2.5	70.9	24.3	2.1	0.2
	FCC	0.2	27.1	69.8	2.7	0.2	0.0

3.3. FCC Multi-Principal-Element Alloys

FCC MPE phases are formed when the difference of the atomic radii between the componential elements are small. The built $6 \times 6 \times 6$ bulk structure models for four- to eight-element FCC MPE phases in this work are presented in Figure 3.

Figure 3. Atomic structure models of four- to eight-element FCC MPE phases by MaxEnt method. The graphs from (**a**) to (**e**) are the quaternary, quinary, senary, septenary, and octonary phases, respectively.

| (a) | (b) | (c) | (d) | (e) |
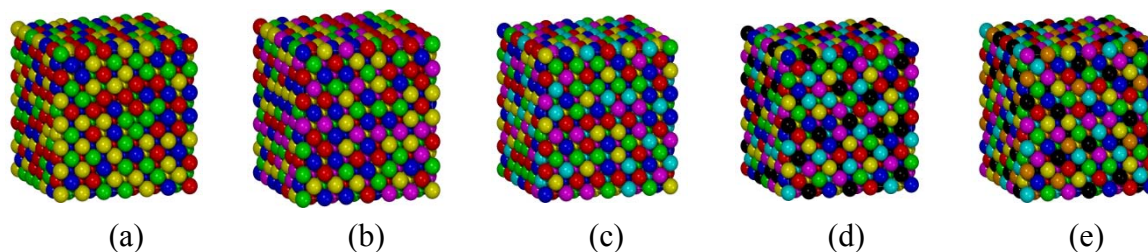
Since the number of atoms in FCC bulk is twice as much as in the BCC phase, it becomes more difficult to separate the same-element atoms. The element distribution analyses given in Table 2 shows that the situation of same-element atoms in the first nearest neighbor is very serious for the quaternary, quinary, and senary FCC MPE phases. The situation gradually improves as the element number increases. The highest frequency of same-element neighboring is at the first nearest neighbor for the first two phases. This peak area moves to the second, and the third nearest neighbors started from the senary, and octonary phases respectively, and only a trace is left in the first nearest neighbor in the octonary phase. Figure 4 shows the atomic structure model of $2 \times 2 \times 2$ quinary FCC MPE phase. There are 63 atoms in the model. The atom numbers of the five different elements are assigned as 13, 13, 13, 12, and 12. It is seen from the figure that some same-element atoms in the first nearest neighborship cannot be avoided because of the limitations in geometry size under this model composition.

Figure 4. Model of $2 \times 2 \times 2$ quinary FCC MPE phase. There are six atoms in blue color, three atoms in yellow color, and two atoms in magenta color in the first nearest neighborship.
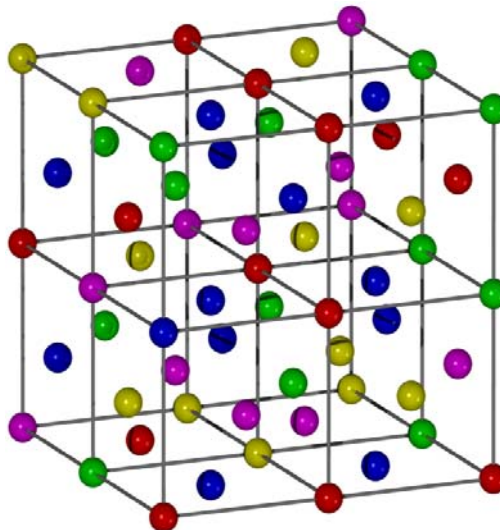
3.4. Applications to the Real Multi-Principal-Element Alloys

Because no direct interatomic interaction was considered in the above modeling work, the built models should subject to further atomic-coordinates optimization [26] by molecular dynamics or first-principles simulations before applying them to the study of various physical properties of the alloys. Applications of the built models to some typical MPE alloys, recently reported by experimental researches, are given in the follows. These alloys are the quaternary FCC FeCoCrNi [9,27], quinary FCC CoCrFeMnNi [28], quinary BCC AlCoCrFeNi [29], and senary BCC AlCoCrCuFeNi [30]. Firstly, the original bulk models of these MPE phases are created from the corresponding MaxEnt models by appropriate elemental substitution. Then, the atomic structures in these models are optimized by Molecular Mechanics simulation by the similar procedure as described in [26]. Chen's lattice inversion pair-function potentials [31] are used to calculate the interatomic interaction in the simulation. The optimized $8 \times 8 \times 8$ bulk structures of these phases are illustrated in Figure 5. The optimized lattice parameters together with the relevant experimental data are listed in Table 3. It was demonstrated that the atomic structure of equimolar multi-component alloys have the 3D paracrystalline lattice configuration [26]. This paracrystalline feature is also reflected in the optimized structure models in Figure 5. The lattice distortion in paracrystals is measured by the lattice distortion parameter g [32], which is defined by:

$$g = \sqrt{\frac{\overline{d^2}}{\overline{d}^2} - 1}.$$ (10)

where, d is a lattice geometrical parameter of the structure, it can be the inter-planar spacing or local lattice parameter; $\overline{d}$ and $\overline{d^2}$ are the mean and square mean values of the lattice geometrical parameter, respectively. The local lattice constant a_l is used in g calculation in this study. The local lattice constant varies due to the lattice distortion in MPE alloys. The calculation method of local lattice constant is illustrated in Figure 6. Parameter g measures the statistical correlation of local lattice constant. The paracrystalline lattice distortion parameters g of these alloys are given in the last column of Table 3. The lattice constant given in this table is the averaged local lattice parameter a_l for all lattice sites in the model. A relatively larger error in the theoretical lattice constant compared to the experimental one of these optimized MPE phases is seen in Table 3. The reason for the problem could be mainly attributed to the empirical interatomic pair-potentials used in the model structure optimization. This problem will be further explored in the discussion section later. The g parameter provides a quantitative evaluation of the lattice distortion in MPE phases, which can be directly measured through x-ray diffraction experiment [32]. There are generally much more serious lattice distortions in BCC MPE alloys than in FCC ones as reflected in Figure 5 and the g parameters in Table 3. The g parameter of BCC MPE alloys is about two to three times higher than that of the FCC ones. The reason for the phenomenon is largely because the atomic radii of the componental elements vary widely in the BCC phases. The degree of lattice distortion in MPE alloy is sensitively depended on its composition as reflected from the calculated g-parameter. There is a close correlation between lattice distortion and the metallic radii [33] of the componental elements. For examples, the FCC phases of FeCoCrNi and CoCrFeMnNi own very small g parameters, which can be explained from the little differences in the metallic radii of

their componental elements: Fe 1.26 Å, Co 1.25 Å, Cr 1.28 Å, Ni 1.24 Å, and Mn 1.27 Å. The metallic radius can be served as an effective criterion for the composition design of MPE alloys.

Table 3. Lattice constant and lattice distortion parameter of the optimized MPE alloys.

Phase	a (Å)	a_{expt} (Å)	Error	g
FCC FeCoCrNi	3.84	3.56 [27]	7.9%	0.0085
FCC CoCrFeMnNi	3.84	3.59 [5]	7.0%	0.0070
BCC AlCoCrFeNi	3.08	2.87 [29]	7.3%	0.0210
BCC AlCoCrCuFeNi	3.10	2.87 [30]	8.0%	0.0150

Figure 5. Relaxed atomic structure models of four typical MPE alloys. The Al, Fe, Co, Cr, Ni, Mn, and Cu atoms are in red, magenta, green, blue, cyan, yellow, and grey colors respectively.

(a) FCC FeCoCrNi

(b) FCC CoCrFeMnNi

(c) BCC AlCoCrFeNi

(d) BCC AlCoCrCuFeNi
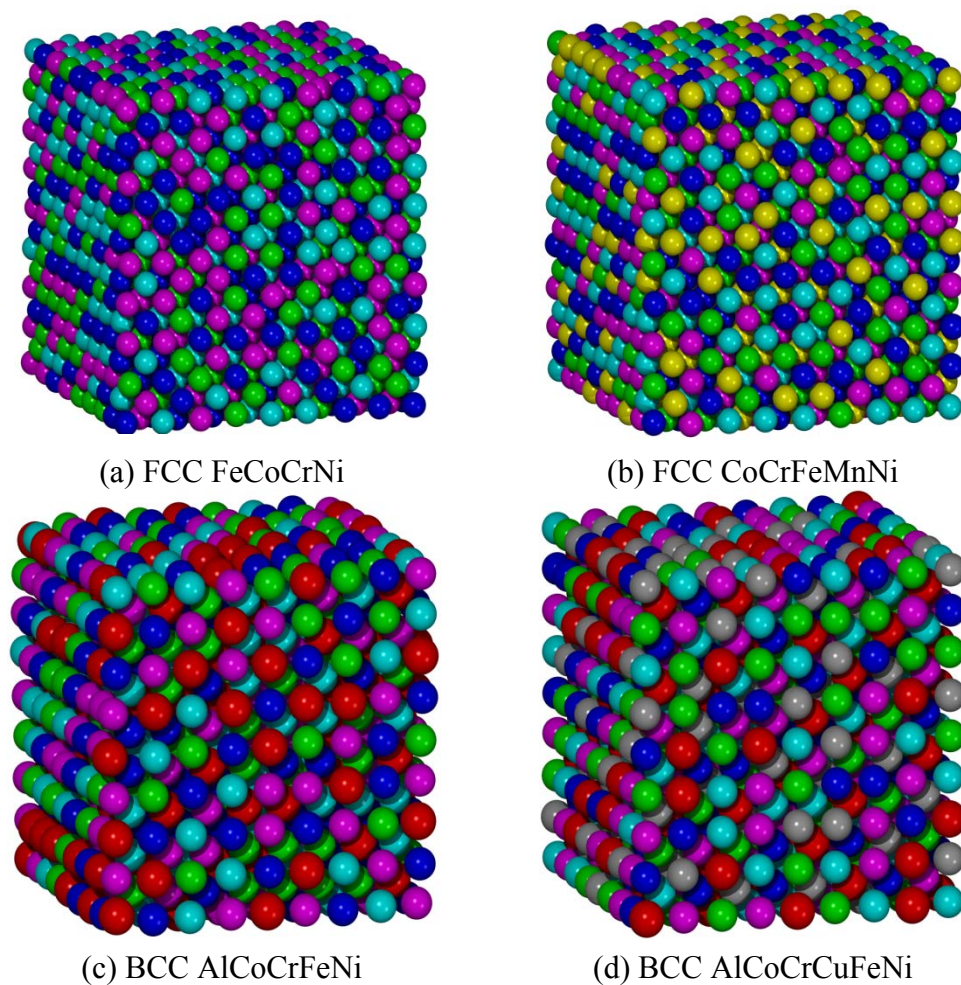
Figure 6. Illustration of the local lattice constant calculation for a deformed cubic cell. The local lattice constant a_l near the yellow atom is calculated by the averaged length of its three neighboring edges $a_l=(a1+a2+a3)/3$ along the three forward axis-directions.
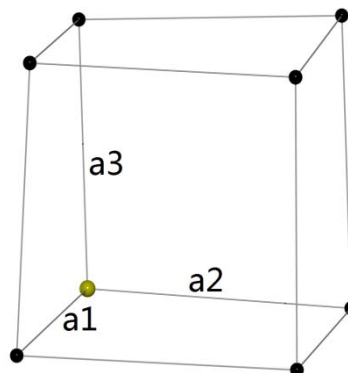
4. Discussion

It could be an impossible task to deduce an explicit expression of entropic force from the definition in Equation (9) because the $v_i(r)$ is correlated with the local environment at position *r*. This situation is similar to the charge density calculation $\rho(r)$ in the density-functional theory. However, the structure optimization can be done by maximizing the spacing of same-type particles since $v_i(r)$ is proportional to the distance of their nearest neighbor. As a rough approximation, the entropic force might be expressed in a similar way as the repulsive Coulomb force of same-type charges in the simulation. The Monte Carlo algorithm is used to search for the system configuration with the maximum distance distribution of same-element atoms in this work. The advantage of this method is that it gives a highly efficient implementation of uniform particles distribution by rapid traversing the entire system space, and thus the time-consuming process of particles diffusion can be avoided. In the physics world, substance is the energy in condensed state, and the behavior of energy is determined by entropy. The in-depth study of entropic force is expected to unify all physics forces, including the electromagnetic force [34,35], gravity [20], *etc.*, and finally leads to the establishment of the Unified Field Theory.

How to accurately modeling the microstructure of the condensed matters with lack of strict periodicity is a long-standing issue in materials research. More difficulty is imposed by the structural description of the random multi-componental systems. Historically, the cluster expansion method [36], the virtual crystal approximation or coherent potential approximation [37], and the special quasi-random structures method [38] were proposed to deal with the local disordered structures seen in the random-substitution alloys. However, none of these methods is sufficient for the structual modeling of MPE alloys, and no success story using these methods in MPE study has been reported yet. MPE alloys receive the name of high-entropy alloys for the high-entropy feature in their structure formation [1]. The maximum-entropy distribution is the most reasonable choice when there are not enough details available in a physical system. MaxEnt is the ideal state of random alloys system in equilibrium. Although the real alloys may deviate from this ideal state due to the diffusion of particles resulting from the local unevenness of physical fields or the special affinity among some elements, the MaxEnt configuration can serve as the reference standard or the starting point for the studies of these real materials. By the MaxEnt principle, there are a great number of MaxEnt configurations for a MPE

alloy. The structure model given in this work is considered as a representative of this total collection. It is expected that the atomic structure modeling study in this work will provide a useful guidance for exploring the relationship between the microstructure and macroscopic properties of MPE alloys.

The advantages for using pair-potentials in the structure optimization of MPE alloys are simplicity, easy creation, and low calculation cost. Almost all the pair-potentials between any two metal elements in the Periodic Table of elements had been created by Chen's lattice inversion method, which is greatly convenient to the studies for the complicated and diverse alloy systems, such as high-entropy alloys. However, these pair-potentials were created from the first-principles total-energy calculation of the relevant unary or binary phases in their ideal stable lattice configurations [31], pair-potentials cannot account for the directional nature of chemical bonds. A considerable error in using these pair-potentials to MPE alloys should be estimated for the quite difference local atomic configurations around the pair atoms in MPE alloys to the creation conditions of these pair-potentials. It should be pointed that there are similar problems in using any other empirical interatomic potentials in the study of MPE alloys. A possible solution to this problem might be the direct first-principles calculation within the framework of density functional theory (DFT). The cost of first-principles calculation is tens of thousands times higher than the empirical potential method. Nevertheless, there are two main difficulties to use DFT calculation in the study of bulk property of MPE alloys: firstly, an efficient DFT calculation is usually realized by the plane-wave pseudo-potentials method which demands a periodic boundary condition, but there is lack of strict periodicity in MPE alloys. The next difficulty is that MPE alloys are composed mainly of transition metal elements, there are still many unsolved problems for how to properly deal with the strong correlations in the localized *f*- and *d*-orbitals in transition elements, even for the most 'state of the art' DFT theory. As a balance between cost and accuracy, the empirical potential calculation could be a reasonable choice in MPE alloy studies.

5. Conclusions

In this paper we have successfully built atomic structure models of multi-principal-element alloys with components ranging from four to eight elements according to the principle of maximum entropy. The principle of maximum entropy predicts a uniform particle distribution in a random-alloy system. With the concept of entropic force, a Monte Carlo method was developed for generating the structure configurations of uniform particle distributions in the models. The lattice geometries of four real MPE alloys are optimized, and their lattice distortion parameters are calculated.

Acknowledgments

Conflicts of Interest

The authors declare no conflict of interest.

References

1. Yeh, J.-W.; Chen, S.-K.; Lin, S.-J.; Gan, J.-Y.; Chin, T.-S.; Shun, T.-T.; Tsau, C.-H.; Chang, S.-Y. Nanostructured high-entropy alloys with multiple principal elements: novel alloy design concepts and outcomes. *Adv. Eng. Mater.* **2004**, *6*, 299–303.
2. Huang, P.-K.; Yeh, J.-W.; Shun, T.-T.; Chen, S.-K. Multi-principal-element alloys with improved oxidation and wear resistance for thermal spray coating. *Adv. Eng. Mater.* **2004**, *6*, 74–78.
3. Clausius, R. Die Energie der Welt ist konstant. Die Entropie der Welt strebt einem Maximum zu. *Annalen der Physik und Chemie* **1865**, *125*, 353–400, (in German).
4. Boltzmann, L. *Lectures on Gas Theory*; University of California Press: Berkeley, CA, USA, 1898.
5. Cantor, B.; Chang, I.T.H.; Knight, P.; Vincent, A.J.B. Microstructural development in equiatomic multicomponent alloys. *Mater. Sci. Eng. A* **2004**, *375*, 213–218.
6. Zhang, Y.; Yang, X.; Liaw, P.K. Alloy design and properties optimization of high-entropy alloys. *JOM* **2012**, *64*, 830–838.
7. Chen, Y.L.; Hu, Y.H.; Tsai, C.W.; Hsieh, C.A.; Kao, S.W.; Yeh, J.W.; Chin, T.S.; Chen, S.K. Alloying behavior of binary to octonary alloys based on Cu-Ni-Al-Co-Cr-Fe-Ti-Mo during mechanical alloying. *J. Alloys Compd.* **2009**, *477*, 696–705.
8. Senkov, O.N.; Wilks, G.B.; Miracle, D.B.; Chuang, C.P.; Liaw, P.K. Refractory high-entropy alloys. *Intermetallics* **2010**, *18*, 1758–1765.
9. Lucas, M.S.; Wiks, G.B.; Mauger, L.; Munoz, J.A.; Senkov, O.N.; Michel, E.; Jorwath, J.; Semiatin, S.L.; Stone, M.B.; Abernathy, D.L.; Karapetrova, E. Absence of long-range chemical ordering in equimolar FeCoCrNi. *Appl. Phys. Lett.* **2012**, *100*, 251907.
10. Shannon, C.E. A mathematical theory of communication. *Bell Sys. Tech. J.* **1948**, *27*, 379–423.
11. Janes, E.T. Information theory and statistical mechanics. *Phys. Rev.* **1957**, *106*, 620–630.
12. Carlsson, A.E.; Fedders, P.A. Maximum-entropy method for electronic properties of alloys. *Phys. Rev.* B **1986**, *34*, 3567–3571.
13. Dobrzynski, L. Maximum-entropy reconstruction of the internal magnetization density distributions in $Fe_3(Al_xSi_{1-x})$ alloys. *J. Phys. Condens. Matter.* **1995**, *7*, 1373–1389.
14. Karlin, H.V.; Gorban, A.N. Maximum entropy principle for lattice kinetic equations. *Phys. Rev. Lett.* **1998**, *81*, 6–9.
15. Sobczyk, K. Reconstruction of random material microstructures: patterns of maximum entropy. *Prob. Eng. Mech.* **2003**, *18*, 279–287.
16. Sankaran, S.; Zabaras, N. A maximum entropy approach for property prediction of random microstructures. *Acta Mater.* **2006**, *54*, 2265–2276.
17. Yonampto, Y. Application of maximum entropy method to semiconductor engineering. *Entropy* **2013**, *15*, 1663–1689.
18. Pecharsky, V.K.; Gschneidner, K.A, Jr. Magnetocaloric effect and magnetic refrigeration. *J. Magn. Magn. Mater.* **1999**, *200*, 44–56.

19. Clusius, K. Origin of zero-point entropy. *Nature* **1932**, *130*, 775–776.
20. Verlinde, E. On the origin of gravity and the laws of Newton. *J. High Ener. Phys.* **2011**, *4*, 29–27.
21. Wissner-Gross, A.D.; Freer, C.E. Causal entropic forces. *Phys. Rev. Lett.* **2013**, *110*, 168702–5.
22. Python Programming Language. Available online: http://www.python.org/ (accessed on 19 September 2013).
23. Numpy. Available online: http://www.numpy.org/ (accessed on 19 September 2013).
24. Martin, G. *Martin Gardner's New Mathematical Diversions from Scientific American*; University of Chicago Press: Chicago, IL, USA, 1983.
25. Song, C.; Wang, P.; Makse, H.A. A phase diagram for jammed matter. *Nature* **2008**, *453*, 629–632.
26. Wang, S.Q. Paracrystalline property of high-entropy alloys. *AIP Adv.* **2013**, *3*, 102105.
27. Lucas, M.S.; Mauger, L.; Munoz, J.A.; Xiao, Y.M.; Sheets, A.O.; Semiatin, S.L.; Horwath, J.; Turgut, Z. Magnetic and vibrational properties of high-entropy alloys. *J. Appl. Phys.* **2011**, *109*, 07E307.
28. Otto, F.; Dlouhy, A.; Somsen, Ch.; Bei, H.; Eggeler, G.; George, E.P. The influences of temperature and microstructure on the tensile properties of a CoCrFeMnNi high-entropy alloy. *Acta Mater.* **2013**, *61*, 5743–5755.
29. Kao, Y.F.; Chen, T.J.; Chen, S.K.; Yeh, J.W.Microstructure and mechanical property of as-cast, -homogenized, and -deformed Al_xCoCrFeNi ($0 \leq x \leq 2$) high-entropy alloys. *J. Alloys Compd.* **2009**, *488*, 57–64.
30. Singh, S.; Wanderka, N.; Murty, B.S.; Glatzel, U.; Banhart, J. Decomposition in multi-component AlCoCrCuFeNi high-entropy alloy. *Acta Mater.* **2011**, *59*, 182–190.
31. Chen, N.X.; Shen, J.; Su, X.P. Theoretical study on the phase stability, site preference, and lattice parameters for Gd(Fe,T)12. *J. Phys. Condens. Matter.* **2001**, *13*, 2727–2736.
32. Hindeleh, A.M.; Hosemann, R. Paracrystals representing the physical state of matter. *J. Phys. C Solid State Phys.* **1988**, *21*, 4155–4170.
33. Greenwood, N.N.; Earnshaw, A. *Chemistry of the Elements*; Butterworth-Heinemann: Oxford, UK, 1997.
34. Wang, T. Coulomb force as an entropic force. *Phys. Rev. D* **2010**, *81*, 104045.
35. Hendi, S.H.; Sheykhi, A. Entropic corrections to Coulomb's law. *Int. J. Theor. Phys.* **2012**, *51*, 1125–1136.
36. Sanchez, J.M.; Ducastelle, F.; Gratias, D. Generalized cluster description of multicomponent systems. *Physica A* **1984**, *128*, 334–350.
37. Jaros, M. Electronic properties of semiconductor alloy systems. *Rep. Prog. Phys.* **1985**, *48*, 1091–1154.
38. Zunger, A.; Wei, S.H.; Ferreira, L.G.; Bernard, J.E. Special quasirandom structures. *Phys. Rev. Lett.* **1990**, *65*, 353–356.
39. POV-Ray Code. Available online: http://www.povray.org (accessed on 19 September 2013).